Signature of Fermi Surface Jumps in Positron Spectroscopy Data

Gh. Adam[a,*), b,†)] and S. Adam[b,‡)]

[a] The Abdus Salam International Centre for Theoretical Physics,
P. O. Box 586, 34100 - Trieste, Italy

[b] Department of Theoretical Physics,
Institute of Physics and Nuclear Engineering
P. O. Box MG-6, RO-76900 Bucharest-Măgurele, Romania

Abstract

A subtractionless method for solving Fermi surface sheets (`FSS`), from measured n-axis-projected momentum distribution histograms by two-dimensional angular correlation of the positron-electron annihilation radiation (`2D-ACAR`) technique, is discussed. The window least squares statistical noise smoothing filter described in Adam *et al.*, NIM A, **337** (1993) 188, is first refined such that the window free radial parameters (`WRP`) are optimally adapted to the data. In an ideal single crystal, the specific jumps induced in the `WRP` distribution by the existing Fermi surface jumps yield straightforward information on the resolved `FSS`. In a real crystal, the smearing of the derived `WRP` optimal values, which originates from positron annihilations with electrons at crystal imperfections, is ruled out by median smoothing of the obtained distribution, over symmetry defined stars of bins. The analysis of a gigacount `2D-ACAR` spectrum, measured on the archetypal high-T_c compound $YBa_2Cu_3O_{7-\delta}$ at room temperature, illustrates the method. Both electronic `FSS`, the ridge along ΓX direction and the pillbox centered at the S point of the first Brillouin zone, are resolved.

*Senior Associate. E-mail: adam@ictp.trieste.it

†Permanent address. E-mail: adamg@roifa.ifa.ro

‡E-mail: adams@roifa.ifa.ro

PACS: 07.05.Kf, 78.70.Bj, 71.18.+y, 74.72.Bk
Keywords: Median smoothing; Least squares smoothing; Positron Annihilation Radiation; Fermi surface; High-T_c superconductivity; $YBa_2Cu_3O_{7-\delta}$.

1 Introduction

While the technique of two-dimensional angular correlation of the positron-electron annihilation radiation (`2D-ACAR`) [1, 2, 3], was successfully used to resolve the Fermi surface topology in various classes of materials (see, e.g., [4] for a recent review), the attempts to use it in high-T_c superconductors met huge difficulties stemming from various sources: the occurrence of a fraction of Fermi electrons which is significantly lower than in normal metals, the layered crystalline structures of the samples, the high proportion of crystal imperfections in the single crystals under investigation.

A straightforward consequence of the occurrence of a layered structure, which prevents the uniform distribution of the thermalized positrons inside the sample, is the limitation of the usefulness of the `2D-ACAR` technique to the resolution of the electronic Fermi sheets only. The occurrence of a small fraction of Fermi electrons results in very weak Fermi surface jumps in the measured momentum density, which can thus be easily missed unless the crystal quality is very high and the accumulated statistics is large enough to get the small Fermi surface jumps resolved.

The resolution of the Fermi surface in high-T_c superconductors is a challenge irrespective of the used technique, however. Each of the techniques used so far (`2D-ACAR`, de Haas-van Alphen, or angle-resolved photoemission spectroscopy (see, e.g., [4] and references quoted therein), has been able to resolve only part of the existing Fermi surface sheets, such that the final representation of the Fermi surface came from the superposition of essentially disjoint pieces of information [5].

In this paper, we consider the identification of the Fermi surface jumps from a `2D-ACAR` histogram which records the projection, along a principal crystallographic axis $\mathbf{n}$, of the momentum density coming from zero-spin positron-electron pairs. Such a histogram will be called thereafter an *n-axis-projected histogram*.

If the single crystal used in a `2D-ACAR` experiment would be perfect, then the statistical noise smoothing by means of an appropriate method (see, e.g., [6, 7, 8]), possibly combined with a method of subtracting the radially

isotropic component, would resolve the characteristic Fermi surface jumps.

In fact, there is an important discrepancy between the experimentally measured and theoretically computed momentum distributions. In the range of low momenta, the latter, which are calculated under the assumption of perfect crystalline periodicity, are found to be sensibly smaller than the former [9]. The origins of this discrepancy have been traced back to the positron annihilation with electrons at crystal imperfections [10, 5]. A quantitative estimate [5] suggested that more than one third of all annihilations belong to this category.

To rule out the spurious effects coming from crystal imperfections, either their contribution is to be explicitly subtracted from the data (as done, e.g., by the Argonne group [10, 5]), or the smoothing method is to be insensitive to the occurrence of crystal imperfections.

Here we report a method of the second kind. There are two basic ingredients of this method: (i) the derivation of *optimally adapted to the data* radial parameters of the constant-weight window least squares (`CW-WLS`) smoothing method reported in [6] and (ii) removal of crystal imperfection dependence of the obtained values by *median smoothing over stars of symmetry relating the bins of the histogram*.

The occurrence of Fermi surface jumps in the data results in jumps in the optimal radial parameters of the `CW-WLS` filter. The presence of crystal imperfections blurs the occurring jumps. The median smoothing restores the jumps, if any.

Essential for the success of such an analysis is the operation of *histogram redefinition from the laboratory frame* (`LF`), $Op_x^D p_y^D p_z^D$, (which is defined by the setup and within which the data acquisition is performed) *to the crystal frame* (`CF`) (which is identified with $\Gamma p_x p_y p_z$, the canonical reference frame of the first Brillouin zone of the crystal [11] and within which the various steps of the off-line analysis of the spectrum are legitimate). Here, this preliminary problem is assumed to be solved along the lines described in [12] Within the procedure described in these papers, the assumption (following from the experiment) of a momentum projection along a principal crystallographic axis is duly checked, such that the expected symmetrization operations are justified and hence the inclusion of *stars* of bins into the smoothing procedure of the median method is a valid operation.

The paper is organized as follows. In Section 2, the `CW-WLS` smoothing method is briefly reviewed and the criteria which serve to the definition of data adapted radial parameters of the smoothing windows are discussed. The

description of the median smoothing is done in Section 3. An illustration on experimental data is reported in Section 4.

2 CW-WLS Statistical Noise Smoothing with Optimal Radial Parameters

2.1 Local smoothing windows

Let $\widetilde{H} = (\widetilde{h}_{ij})$ denote the raw LF 2D-ACAR histogram of interest, corrected for finite detector aperture and local variations of the detector sensibility [6]. The statistically relevant information within $\widetilde{H}$ *sharply decreases* when one goes from the histogram center towards its borders. This feature is preserved in the CF histogram $H = (h_{kl})$, obtained from $\widetilde{H}$ under proper discretization in the $\Gamma p_x p_y p_z$ frame [12].

As a consequence, the histogram bins can be divided into two classes: *central* and *border* bins. The separation line between the two bin classes is somewhat arbitrary. For instance, if we decide to restrict the analysis to the projection of the first Brillouin zone onto the histogram plane (1BZ), then the central bin area has to include both 1BZ and a surrounding neighborhood of it, half 1BZ wide say, to get detailed information on the momentum distribution around both sides of the 1BZ boundaries. If, however, the decision is taken to include the maximum possible histogram area into analysis, an appropriate definition of the central bin manifold includes the largest possible histogram area D_Λ related by a similarity transform, of factor $(2\Lambda+1)\times(2\Lambda+1)$ to the D_0 area of 1BZ. (Typically, Λ equals two or three, depending on the setup.)

In [6], a least squares fit of noise-free data to the noisy H data was proposed to be performed, at the fractionary coordinates (ξ, η) of interest inside *each* (K, L)*-th central bin* (where the quantities ξ and η may vary from bin to bin), by means of *local approximating surfaces*, C_{KL}, characterized by the following two features:

1. Each C_{KL} is to consist of an integer number of bins. (This requirement follows from the *data discretization* into square bins, that is, into finite regions inside which the structural details of the momentum distribution have been averaged out — and hence lost — within the process of data acquisition. The bin size a_D is taken henceforth for the unit length of the distances in the histogram plane.)

2. In the limit of an in-plane *continuous* point distribution, the approximating surface C_{KL} is to be *circular* around the point of coordinates (K, L). (Such a choice shows the *largest linear dimensions under the smallest area* and it fits *isotropically* the various possible neighbourhoods. It is thus expected to secure, among the possible `2D` shapes, the *least* L_2 norm departure from *arbitrary* input surfaces.)

As a consequence, to perform statistical noise smoothing, we draw around *each* (K, L)*-th central bin* a *smoothing window* C_{KL} of *quasi-circular shape* which includes inside it all the bins the centres (κ, λ) of which satisfy the inequality

$$(\kappa - K)^2 \ + \ (\lambda - L)^2 \ \leq \ (2r + 1)^2/4, \tag{1}$$

where the quantity r denotes the *window radial parameter*.

2.2 `CW-WLS` smoothing formula

To accommodate both the data discretization into bins and the possibility to predict noise-free values *inside the bins*, the approximating space of noise-free data is spanned by a basis set of polynomials of continuous variables, $P_m(x, y)$, orthogonal over C_{KL}. In what follows, it is assumed that the basis polynomials are of at most 3-rd degree in each of the variables x and y.

Over a local window C_{KL}, the standard deviations $\sigma_{K+k,L+l}$ associated to the elements $h_{K+k,L+l}$, $(K + k, L + l) \ \in \ C_{KL}$ of H show little variation from σ_{KL}, the standard deviation of h_{KL} at the center of the window [6, 13]. We may therefore assume *constant bin weights*, $\sigma_{K+k,L+l} = \sigma_{KL}$, within each smoothing window (1), a hypothesis which results in a *constant weight* `WLS` *smoothing formula* of radial parameter r (`CW-WLS`(r)).

At the fractionary coordinates (ξ, η) inside the (K, L)-th bin,

$$-\,0.5 \ \leq \ \xi \ \leq \ 0.5, \quad -\,0.5 \ \leq \ \eta \ \leq \ 0.5, \tag{2}$$

the `CW-WLS`(r) yields a smoothed value

$$s_{K+\xi,L+\eta} \ = \ \sum_{K+k,L+l \in C_{KL}} h_{K+k,L+l} \ G(\xi, \eta; k, l), \tag{3}$$

where the *Green matrix* of the smoothing formula is given by

$$G(\xi, \eta; k, l) \ = \ \sum_{m=0}^{M} \ \nu_m^2 \ J_{0m}(k, l) \ P_m(\xi, \eta). \tag{4}$$

Here, ν_m denotes the norm of the m-th polynomial P_m over its definition area C_{KL}, while $J_{mm'}(k,l)$, the overlap integral of the basis polynomials $P_m(x,y)$ and $P_{m'}(x,y)$ over the area of the (k,l)-th relative bin inside the current smoothing window. For a set of basis polynomials of at most 3-rd degree, the upper summation index in Eq. (4) is $M = 10$.

2.3 Optimal values of the window radial parameters

To achieve the *best data fit* over an *admissible class* of functions, a consistent least squares fit procedure involves two kinds of *free parameters:* (i) the fit parameters which secure minimum L_2 norm departure of the data from a *particular function* belonging to the admissible class, and (ii) the free parameter which selects the *best function within the admissible class*. The difficult point is to fix the last parameter of the procedure.

The `CW-WLS` procedure for statistical noise smoothing described in [6] and summarized above solves the problem (i) (i.e., it defines the best parameters of the *constant polynomial degree* smoothing filter (3) under a given radial parameter, r, Eq. (1)). The solution of problem (ii), which consists in the definition of the *best* r value, that is of the most suitable smoothing window C_{KL} under an existing neighborhood of the reference bin (K,L), will be discussed below.

Within the usual *polynomial fit*, which adjusts a polynomial function of *variable degree* to an input set consisting of a *fixed* number of elements, to get the *best polynomial degree*, the method starts with a low polynomial degree which is then gradually increased by unity until a stopping criterion is satisfied.

Of interest for the present investigation is the criterion proposed by Hamming [14]. Considering one-dimensional data, Hamming recommends the definition of the best polynomial degree from the *study of the distribution of the signs of the residuals* of the smoothed data. When the polynomial degree is increased, a threshold value is reached at which the signs of the residuals over the set under study show *stochastic distribution* (i.e., the residuals mainly consist of statistical noise), while at higher polynomial degrees, the *prevalence of a given sign* over the set of residuals is obtained (that is, a significant part of the useful signal is chopped by the smoothing polynomial). The threshold defines the degree of the best fit polynomial.

While the problem considered by Hamming is different from the present one, its principle is very well suited to the definition of the radial parameter,

r, Eq. (1). Thus, instead of varying the degree of the smoothing surface, we *adjust its extension* by variable r values in a range $\{r_{min}, r_{max}\}$. We choose $r_{min} = 2$, which is the lowest available radial parameter value for the window (1), while $r_{max} = 13$, a value which corresponds to the chopping of the most part of the useful signal by the smoothing procedure. A threshold value results, $r_{opt} \in \{r_{min}, r_{max}\}$, with similar properties to those of the best polynomial degree within Hamming's procedure.

The residual of the smoothed value (3) at the fractionary (ξ, η) coordinates inside the $(K + k, L + l)$-th bin belonging to the window C_{KL}, Eq. (1) is, by definition,

$$\delta_{K+k+\xi,L+l+\eta} = s_{K+k+\xi,L+l+\eta} - h_{K+k,L+l}. \tag{5}$$

Given a C_{KL} window, signs of quantities (5) are computed over two-dimensional submanifolds of it which obey to two requirements: the submanifolds have to be large enough such as to result in statistically relevant information on the distribution of the signs of the residuals around the reference bin, while low enough to secure a sufficiently fast algorithm.

The least possible manifold of interest is $V_1(K, L)$, the neighborhood of the (K, L)-th bin which consists of the reference bin and its eight nearest neighbors. If *all* the nine signs entering $V_1(K, L)$ are *identical* with each other, then the distribution is assumed to be non-stochastic.

If this rule fails, then we consider the larger neighborhood $V_2(K, L)$ of the (K, L)-th bin, defined by the 21 bins of the C_{KL} window (1) at the radial parameter value $r = r_{min} = 2$. If *two-thirds* at least of the signs of the residuals inside $V_2(K, L)$ are *identical*, then the statistics is assumed to be non-stochastic.

These two sign count criteria following from Hamming's procedure, however, do not exhaust the manifold of non-stochastic two-dimensional distributions. There is still the possibility of ordered sign distributions characterized by nearly equal occurrence of positive and negative signs. To pick them out, the analysis of *directional sign distribution* of the residuals inside $V_2(K, L)$ is performed along one or several of the following four directions: the p_x axis, the p_y axis, the first bisectrix, and the second bisectrix. In each case, we count the *ordered triplets*, i.e., the sets of *identical three signs at neighboring bins* along rows, columns, or diagonals respectively. If the count yields a *majority of ordered triplets* with respect to the total number of possible ordered triplets in the considered direction, then we decide that the sign distribution is non-stochastic.

An *accidental fulfillment* of one of the three abovementioned criteria is possible, with the consequence that a spurious r_{opt} cutoff is obtained. To avoid such a premature end of the analysis, the requirement of *preservation* of the non-stochasticity of the sign distribution within $V_1(K,L)$ or $V_2(K,L)$ under further increase of the radial parameter r is imposed.

Within an ideal, perfect single crystal, the occurrence of jumps in the optimal radial parameters closely follows the characteristic Fermi surface jumps in the measured momentum distribution. Unfortunately, the real single crystals show a great many number of imperfections of various kinds, which significantly alter the obtained optimal window radial parameters. The crystal imperfections blur the Fermi surface jump pattern and make it indistinguishable from a stochastic momentum distribution. Thus, in real crystals, the abovementioned definition of the optimal window parameters is to be supplemented with a procedure able to restore the jumps at contiguous bins which are characteristic to the Fermi surface.

Such a procedure is discussed in the next section.

3 Elimination of Spurious Impurity Effects by Median Smoothing

The median smoothing is known to *preserve the jumps*, if any, within the distribution under consideration. Consistent median smoothing of physical quantities associated to an n-axis-projected histogram, H, is obtained provided the following two distinct problems are correctly solved. The first concerns the *parameters* of the two-dimensional smoothing window: *the extension of the neighborhood* of the (K,L)-th bin over which the median smoothing is to be done and the *weights* assigned to the bins entering this neighborhood. The second concerns the *symmetry induced relationships* among the bins of the histogram. Each of these problems is considered in detail below.

The *extension of the neighborhood* entering the median smoothing of the (K,L)-th bin can be chosen to be either a $V_1(K,L)$ or a $V_2(K,L)$ neighborhood (defined in Sec. 2.3 above).

Within a $V_1(K,L)$ neighborhood, it is natural to assume *equal weights* to all the bins entering it:

$$\begin{pmatrix} 1 & 1 & 1 \\ 1 & 1 & 1 \\ 1 & 1 & 1 \end{pmatrix} \tag{6}$$

Within an $V_2(K,L)$ neighborhood, we can either assume *equal bin weights*

$$\begin{pmatrix} 0 & 1 & 1 & 1 & 0 \\ 1 & 1 & 1 & 1 & 1 \\ 1 & 1 & 1 & 1 & 1 \\ 1 & 1 & 1 & 1 & 1 \\ 0 & 1 & 1 & 1 & 0 \end{pmatrix} \tag{7}$$

or we can assume *different weights*. Here we consider the hat shape

$$\begin{pmatrix} 0 & 1 & 2 & 1 & 0 \\ 1 & 3 & 5 & 3 & 1 \\ 2 & 5 & 8 & 5 & 2 \\ 1 & 3 & 5 & 3 & 1 \\ 0 & 1 & 2 & 1 & 0 \end{pmatrix} \tag{8}$$

In the case of data characterized by a high level of crystal imperfections, the neighborhood $V_1(K,L)$ with equal weights (6) is too small to result in effective cut of the fluctuations residing in the imperfections. The neighborhood $V_2(K,L)$ with equal weights (7) is also inappropriate since it overemphasizes the far staying bins, while the weight of the reference bin is negligibly small. The most adequate seems to be the choice $V_2(K,L)$ with unequal weights (8) which includes sufficient enough neighbors while securing a fifty-fifty ratio between the weights assigned to the reference bin and its nearest neighbours on one side and the farther staying bins on the other side.

Since the information stored in different bins comes from a crystal, there are strong symmetry induced correlations of the Fermi-surface-related information stored in a `2D-ACAR` histogram. As a consequence, our smoothing method has to be able to emphasize it. To implement this aspect into the median smoothing, we make reference to the Neumann principle (see, e.g., [15]), according to which, the symmetry originating in positron annihilations with electrons within bands crossing the Fermi level, is a subduction to the histogram plane of the symmetry point group of the reciprocal lattice of the crystal.

For an n-axis-projected `2D-ACAR` histogram of interest here, the distinct symmetry elements characterizing this electron fraction are: the *inversion symmetry center* Γ (placed at the zero-momentum projection of the distribution), a *rotation axis* along $\mathbf{n}$, and in-plane *symmetry lines*.

The occurrence of the symmetry classifies the various bins entering an n-axis-projected `CF` histogram H into *stars of symmetry*. In the case of an $YBa_2Cu_3O_{7-\delta}$ single crystal for instance, the stars of the bins entering both the c-axis-projected and a-axis-projected histograms contain one, two, or four elements, according to the fact that the bin of interest contains the symmetry inversion center Γ inside it, or it lies along a symmetry axis, or it is a general bin.

In conclusion, there are three essential steps which secure the correct approach to the median smoothing of an n-axis-projected `2D-ACAR` histogram:

- Derivation of the `CF` histogram H from the `LF` histogram $\widetilde{H}$;
- Derivation of the window optimal radial parameters;
- Median smoothing over manifolds of data consisting of symmetry stars of bins, within neighborhoods V_2, with bin weights (8).

Such a procedure finally yields window optimal radial parameters characteristic to a structure showing the n-axis-projection of the Fermi surface of the sample. As a consequence, if the accumulated statistics contains characteristic Fermi surface jumps indeed, then the procedure should be able to put them into evidence as *characteristic jumps* in the final window optimal radial parameters. That is, while a Fermi-surfaceless structure is characterized by *gradual* variations of the window radial parameters (i.e., δr jumps between neighboring bins in the range {-1, 0, 1}), the occurrence of lines of Fermi surface within the `2D` momentum projection should be evidenced by jumps $|\delta r| \geq 2$ *at contiguous bin positions*.

The next section illustrates this feature on a set of data open to contradictory interpretation within the usual off-line processing methods.

4 Results and Their Discussion

The use of the present method is illustrated on a c-axis-projected `2D-ACAR` histogram labelled "580", measured on an $YBa_2Cu_3O_{7-\delta}$ single crystal, at room temperature, at the University of Geneva, with an upgraded version of the setup described in [16] and previously analyzed with different methods of resolving the anisotropic component of the `2D-ACAR` spectrum [6, 12, 17, 18, 19].

The parameters which define the crystal frame $\Gamma p_x p_y p_z$ within the laboratory frame $O p_x^D p_y^D p_z^D$ are

$$\{\widetilde{\gamma}_x = \kappa_0 + \xi_0, \quad \widetilde{\gamma}_y = \lambda_0 + \eta_0, \quad \phi_0, \quad \theta_0, \quad \psi_0\}. \tag{9}$$

Here $(\widetilde{\gamma}_x, \widetilde{\gamma}_y)$ denote the in-plane Γ coordinates, while ϕ_0, θ_0, ψ_0 are the Euler angles which define the rotations from the $O p_x^D p_y^D p_z^D$ frame axes to the $\Gamma p_x p_y p_z$ frame axes.

The rough approximations (κ_0, λ_0), to the coordinates of Γ have been found to be $(-1.0, 5.0)$, while the fractionary coordinates were found to be $\xi_0 = -0.1146 \times 10^{-1}$ and $\eta_0 = 0.2413$ (in a_D units). The value of the Euler angle θ_0 was found to be negligibly small ($\theta_0 = -0.316 \times 10^{-3}$ radians), such that the experimental histogram can be accepted for a c-axis-projected histogram indeed. Then the only relevant Euler angle is the sum of the angles ϕ_0 and ψ_0, $\alpha_0 = -0.12297 \times 10^{-2}$ radians.

The final result of the procedure described in the previous sections is shown in figure 4. Both the electron ridge crossing the first Brillouin zone from Γ to X and the pillbox around the S corners are resolved. It is to be stressed that the ridge-jumps have been of high amplitude (δr inbetween three to six units large), while the pillbox-jumps have always been characterized by the minimal $\delta r = 2$ value, telling us that the collected ridge jump signal is strong, while the pillbox jump signal is weak.

Whereas the occurrence of the Fermi surface ridge in the analyzed "580" histogram was confirmed by different signal processing techniques in all the five references mentioned above, [6, 12, 17, 18, 19]. the only references which analyze the pillbox are [19] and [12].

The methods of analysis used in [19]) did not confirm the occurrence of the pillbox in $YBa_2Cu_3O_{7-\delta}$ at room temperature. The measurements of the positron mean free path in this compound at different temperatures suggested that, at room temperature, there is a shallow positron trapping mechanism which is responsible of the absence of the pillbox.

Our previous analysis of the same spectrum [12] has found that the resolved pillbox exists, but it is small (the depth of the Lock-Crisp-West (`LCW`) folded [20] signal at the S point was found to be only four times larger than the experimental errors).

The present investigation, which is not symmetric component subtraction sensitive, adds considerable weight to the conclusions of reference [12], without making use of the `LCW` folding to achieve signal enhancement. It lets

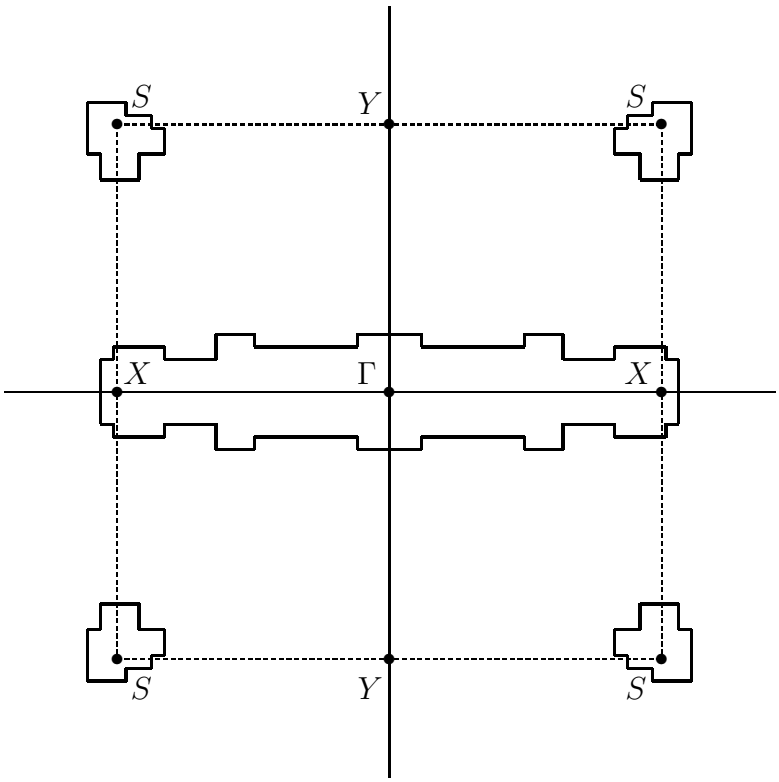

Figure 1: Occurrence of jumps of the window optimal radial parameters of the `CW-WLS` method for statistical noise smoothing resolves two Fermi surface sheets: the *ridge*, going from Γ to X across the whole first Brillouin zone of the sample and the *pillboxes*, around the corners S of the first Brillouin zone.

us infer that, while weakening considerably the pillbox signature at room temperature indeed, the positron shallow trapping does not rule it out altogether. It is to be noted, however, that, although describing a closed contour jump in the measured positron-electron momentum distribution, the shape of the resolved pillbox around the S point is irregular, a feature which tells us about is small amplitude, which can be easily distorted by the occurrence of non-homogeneously distributed crystal defects.

5 Acknowledgments

We are very much indebted to Professor Martin Peter from the University of Geneva, Switzerland, who introduced us to the field of positron spectroscopy. Discussion with him and with Professor Alfred A. Manuel from Geneva University at various stages of the investigation, as well as provision of the experimental data, are gratefully acknowledged.

Part of this work was done within the framework of the Associateship Scheme of the Abdus Salam International Centre for Theoretical Physics, Trieste, Italy. The first author would like to thank Professor M. Virasoro and the Abdus Salam ICTP for hospitality and for granting him generous access to the computing facilities of the Centre.

The work done in Romania was financed by the Ministry of Research and Technology of Romania.

References

[1] S. Berko, in: Positron Solid State Physics, Proc. of the Int. School "E. Fermi", Course 83, W. Brandt and A. Dupasquier eds., (North Holland, New York, 1983) pp. 64–145. Reprinted in Positron Studies of Solids, Surfaces and Atoms, A.P. Mills,Jr., W.S. Crane and K.F. Canter eds., (World Scientific, Singapore, 1986) pp. 246–327.

[2] S.Berko, in: Momentum Distributions, R.N. Silver and P.E. Sokol eds., (Plenum Press, New York, 1989) p. 273.

[3] M. Peter, IBM J. Res. Develop. 33/3 (1989), 333.

[4] L.P. Chan, K.G. Lynn and D.R. Harshman, Mod. Phys. Lett. B, 6 (1992), 617, and references therein.

[5] R. Pankaluoto, A. Bansil, L.C. Smedskjaer and P.E. Mijnarends, Phys. Rev. B, 50 (1994), 6408.

[6] Gh. Adam, S. Adam, B. Barbiellini, L. Hoffmann, A.A. Manuel and M. Peter, Nucl. Instr. and Meth. A, 337 (1993), 188.

[7] L. Hoffmann, A. Shukla, M. Peter, B. Barbiellini and A.A. Manuel, Nucl. Instr. and Meth. A, 335 (1993), 276.

[8] R.N. West, in: Positron Spectroscopy of Solids, A. Dupasquier and A.P. Mills, Jr. eds., (North Holland, New York, 1995).

[9] L. Hoffmann, W. Sadowski, A. Shukla, Gh. Adam, B. Barbiellini, and M. Peter, J. Phys. Chem. Sol. 52 (1991), 1551.

[10] L.C. Smedskjaer, A. Bansil, U. Welp, Y. Fang and K.G. Bailey, Physica C, 192 (1992), 259.

[11] C.J. Bradley and A.P. Cracknell, The Mathematical Theory of Symmetry in Solids: Representation Theory for Point Groups and Space Groups (Clarendon Press, Oxford, 1972).

[12] Gh. Adam and S. Adam, International J. Modern Phys. B, 9 (1995), 3667.

[13] Gh. Adam and S. Adam, Romanian J. Phys., 38 (1993), 681.

[14] R. W. Hamming, Numerical Methods for Scientists and Engineers, 2-nd ed. (Mc Graw-Hill, New York, 1973), Chaps. 25–27.

[15] R.R. Birss, Symmetry and Magnetism (North-Holland, Amsterdam, 1964).

[16] P.E. Bisson, P. Descouts, A. Dupanloup, A.A. Manuel, E. Perreard, M. Peter and R. Sachot, Helv. Phys. Acta 55 (1982), 100.

[17] Gh. Adam, S. Adam, B. Barbiellini, L. Hoffmann, A.A. Manuel, M. Peter and S. Massidda, Solid State Commun. 88 (1993), 739.

[18] L. Hoffmann, A.A. Manuel, M. Peter, E. Walker, M. Gauthier, A. Shukla, B. Barbiellini, S. Massidda, Gh. Adam, S. Adam, W.N. Hardy, Ruixing Liang, Phys. Rev. Lett. 71 (1993), 4047.

[19] A. Shukla, L. Hoffmann, A.A. Manuel, E. Walker, B. Barbiellini, and M. Peter, Phys. Rev. B 51 (1995), 6028.

[20] D.G. Lock, V.H.C. Crisp and R.N. West, J. Phys. F: Metal Phys. 3 (1973), 561.